HHS Public Access

Author manuscript

Nat Neurosci. Author manuscript; available in PMC 2016 April 20.

Published in final edited form as:

Nat Neurosci. 2016 January ; 19(1): 65–74. doi:10.1038/nn.4193.

Oligodendrocyte death results in immune-mediated CNS demyelination

Maria Traka[1,3], **Joseph R Podojil**[2,3], **Derrick P McCarthy**[2], **Stephen D Miller**[2], and **Brian Popko**[1]

[1]Department of Neurology, The University of Chicago Center for Peripheral Neuropathy, The University of Chicago, Chicago, Illinois, USA.

[2]Department of Microbiology-Immunology and Interdepartmental Immunobiology Center, Northwestern University Feinberg School of Medicine, Chicago, Illinois, USA.

Abstract

Although multiple sclerosis is a common neurological disorder, the origin of the autoimmune response against myelin, which is the characteristic feature of the disease, remains unclear. To investigate whether oligodendrocyte death could cause this autoimmune response, we examined the oligodendrocyte ablation *Plp1-CreER^{T};ROSA26-eGFP-DTA* (DTA) mouse model. Approximately 30 weeks after recovering from oligodendrocyte loss and demyelination, DTA mice develop a fatal secondary disease characterized by extensive myelin and axonal loss. Strikingly, late-onset disease was associated with increased numbers of T lymphocytes in the CNS and myelin oligodendrocyte glycoprotein (MOG)-specific T cells in lymphoid organs. Transfer of T cells derived from DTA mice to naive recipients resulted in neurological defects that correlated with CNS white matter inflammation. Furthermore, immune tolerization against MOG ameliorated symptoms. Overall, these data indicate that oligodendrocyte death is sufficient to trigger an adaptive autoimmune response against myelin, suggesting that a similar process can occur in the pathogenesis of multiple sclerosis.

Multiple sclerosis (MS) is an autoimmune inflammatory disease in which T cells attack the myelin sheaths of nerves in the CNS, resulting in neuronal dysfunction[1]. In most patients, MS initiates as a relapsing-remitting neurological disorder that over time advances to a chronic progressive disease characterized by the accumulation of neurological deficits. Although MS has long been considered an inflammatory neurodegenerative disease, its etiology is not well understood[2]. The principal ‘outside-in’ hypothesis for MS pathogenesis centers on the idea that primary dysregulation of the immune system leads to autoreactivity

Correspondence should be addressed to S.D.M. (s-d-miller@northwestern.edu) or B.P. (bpopko@uchicago.edu).

[3]These authors contributed equally to this work.

AUTHOR CONTRIBUTIONS

M.T. and J.R.P. designed the studies, performed the experiments, analyzed and interpreted the data and wrote the manuscript. D.P.M. assisted with the induction and completion of the $MOG_{35–55}$ specific tolerance experiments. B.P. and S.D.M. supervised the project, assisted with experimental design, data interpretation and manuscript preparation.

COMPETING FINANCIAL INTERESTS

The authors declare no competing financial interests.

against myelin-sheath components[3,4], which secondarily leads to breakdown of the blood–brain barrier. This is followed by infiltration of the CNS by T cells, leading to the focal inflammation and demyelination that characterize MS lesions[3].

An alternative, 'inside-out' hypothesis is based on pathological evidence showing that oligodendrocyte loss[5,6] and myelin defects[7] occur in the brains of patients with MS even in the absence of apparent signs of inflammation. Thus, the loss of oligodendrocytes and subsequent demyelination might result in autoreactivity against myelin antigens and, secondarily, lead to inflammation and demyelination in the CNS. We explored this possibility using our previously established *Plp1-CreER^T;ROSA26-eGFP-DTA* (DTA) mouse model, in which oligodendrocytes are killed in adult mice by the genetic activation of diphtheria toxin fragment A expression[8]. *Plp1-CreER^T* mice express the Cre recombinase fused to the mutant human estrogen receptor (ER^T) in oligodendrocytes under the transcriptional control of the myelin proteolipid protein (*Plp1*) gene[9]. The recombinase activity of CreER^T is stimulated by tamoxifen[10], which allows the inducible recombination of the *ROSA26-eGFP-DTA* locus, resulting in the diphtheria toxin–mediated ablation of oligodendrocytes[8]. Here we show that the initial oligodendrocyte loss is followed by infiltration of CD4$^+$ T cells into the CNS, which leads to a secondary, fatal demyelinating disease later in life. Late-onset demyelination in DTA mice was accompanied by axonal loss and coincided with CNS inflammation and the presence of myelin-specific ($MOG_{35–55}$-specific) T cells in peripheral lymphoid organs. It therefore seems likely to be a T cell–mediated autoimmune response. This theory is supported by two main findings: first, adoptive transfer of the myelin-specific DTA-derived T cells into naive mice consistently resulted in the induction of mild neurological symptoms and inflammatory CNS white matter lesions in the recipient animals; and second, induction of immune tolerance to the $MOG_{35–55}$ peptide inhibited the progression of late-onset disease symptoms in DTA animals. To our knowledge, this is the first experimental evidence to support the hypothesis that oligodendrocyte loss or myelin degeneration triggers myelin autoimmunity and initiates inflammation and tissue damage in the CNS during MS.

RESULTS

Late-onset CNS demyelination and immune activation in DTA mice

As we previously described[8], after tamoxifen injection to activate diphtheria toxin expression in myelinating cells, severe neurological symptoms are seen in DTA mice that correlate with wholesale oligodendrocyte loss and widespread CNS demyelination, which peak 5 weeks after injection. Affected mice recover from most clinical symptoms by 10 weeks after injection, owing to repopulation of oligodendrocytes and substantial remyelination[8]. Nevertheless, we subsequently observed that all recovered tamoxifen-treated DTA mice developed secondary, late-onset neurological symptoms starting around 40 weeks after injection, including severe ataxia (Supplementary Movie 1), impaired motor skills (Fig. 1a), weight loss (Fig. 1b) and seizures. Approximately 50% of these mice were dead 52

Any Supplementary Information and Source Data files are available in the online version of the paper.

weeks after injection, whereas control littermate (*ROSA26-eGFP-DTA*) mice developed no symptoms.

Histological analysis of CNS pathology 40 weeks after injection revealed the presence of focal lesions in the brainstem, cerebellum and cervical spinal cord of the tamoxifen-treated DTA mice. These white matter lesions were identified by their lighter staining on sections stained with hematoxylin and eosin (Fig. 2a). Toluidine blue staining and electron microscopy (EM) analyses of the focal lesions showed the presence of macrophages containing myelin debris (Fig. 2b,c) and unmyelinated axons (Fig. 2c), indicating ongoing demyelination. The focal lesions were negative for myelin basic protein (MBP) staining (Fig. 2d) and appeared to be sites of active inflammation: they were frequently infiltrated by T cells (Fig. 2d), and they contained a high density of microglia or macrophages (Fig. 2d) and, in the cerebellum, unmyelinated axons (Fig. 2d). Quantitative analysis showed that the focal lesions were rare in the DTA mice 40 weeks after injection: we found on average 2 ± 1 lesions in the cerebellar white matter, 2 ± 2 lesions in the cervical spinal cord white matter and 3 ± 1 lesions in the brainstem white matter by examining hematoxylin and eosin–stained brain sections (~20 sagittal, 10 μm thick) and cervical spinal cord sections (~20 horizontal, 10 μm thick) from these mice ($n = 3$ mice). No focal white matter lesions were observed in the CNS of control littermate (*ROSA26-eGFP-DTA*) mice or untreated DTA mice (data not shown). At 1 year after injection, focal lesions were no longer detected in the cerebellum, corpus callosum, cervical spinal cord or brainstem of the tamoxifen-treated DTA mice. These animals did, however, display widespread myelin loss on toluidine blue–stained sections (Fig. 3a) and by EM analysis (Fig. 3b). Late-onset demyelination in these animals was not associated with substantial loss of oligodendrocytes or neurons in any CNS areas except the brainstem, which showed an approximate 50% decrease in cells stained for the oligodendrocyte marker CC-1 (Fig. 3c). Quantification of the neuronal biomarker NeuN revealed that there were normal numbers of neurons in the brainstem and the cervical spinal cord (data not shown). Nevertheless, late-onset demyelination significantly affected axonal survival in the DTA animals: counts showed significant axonal loss in the ventrolateral white matter of the cervical spinal cord (~40%) and the optic nerve (~55%) (Fig. 3d). A similar diminution in axon numbers was not observed in the tamoxifen-treated DTA mice following recovery from the acute demyelinating disease[8].

Although our previous data showed that the adaptive immune system was not activated at the peak of oligodendrocyte loss (5 weeks after injection) in tamoxifen-treated DTA mice[8], the late-onset demyelination in these animals was associated with T cell inflammation in the CNS. Staining for the T cell marker CD3 showed increased numbers of $CD3^+$ T cells 53 weeks after injection in the tamoxifen-treated DTA mice (Supplementary Fig. 1). Notably, similar analyses also showed increased numbers of $CD3^+$ T cells in the CNS of tamoxifen-treated DTA mice as early as 7 weeks after injection (data not shown), when the mice had started recovering from the initial oligodendrocyte loss. Flow cytometry 10 and 40 weeks after injection revealed that the number of $CD4^+$ T cells present in the CNS of tamoxifen-treated DTA mice was significantly higher than that in control littermates (*ROSA26-eGFP-DTA*) (Fig. 4a,b). Additionally, at 40 weeks after injection, the number of $MHCII^+B7^+$ ($CD80^+CD86^+$) dendritic cells was significantly higher in tamoxifen-treated DTA mice than in control mice (Fig. 4b). Dendritic cells represent the main CNS antigen-presenting cell

type during $CD4^+$ T cell–induced inflammatory demyelinating response in a mouse model of MS, experimental autoimmune encephalomyelitis (EAE)[11]. Therefore, activated $CD4^+$ T cells are present in the CNS as early as 10 weeks after injection, and both activated $CD4^+$ T cells and antigen-presenting dendritic cells are present in the CNS 40 weeks after injection.

Flow cytometry analysis 40 weeks after injection, to investigate whether myelin-specific $CD4^+$ T cell responses were quantifiable in the spleens and cervical lymph nodes of tamoxifen-treated DTA mice, indicated that there was no statistical difference in the number of $CD4^+$ T cells, $CD8^+$ T cells, B cells, monocytes and dendritic cells present in the spleen of tamoxifen-treated DTA mice compared with controls (Fig. 4c). The total numbers of $CD4^+$ T cells, $CD8^+$ T cells, B cells, monocytes and dendritic cells in the CNS-draining cervical lymph nodes of tamoxifen-treated DTA mice were significantly higher than in those of the controls (Fig. 4d). In contrast to findings 10 weeks after injection (data not shown), at 40 weeks after injection autoreactive T cells capable of proliferating in response to stimulation with recombinant rat MOG protein were seen in the spleen and cervical lymph nodes, and autoreactive T cells capable of proliferating in response to stimulation with the immunodominant $MOG_{35–55}$ epitope were found in the spleen (Fig. 4e,f). No responses to the C57BL/6 (MHC II allele $I\text{-}A^b$)-restricted $PLP_{178–191}$ or SJL/J (Swiss Jim Lambert/Jackson) ($I\text{-}A^s$)-restricted $PLP_{139–151}$, $MBP_{84–104}$ or ovalbumin peptide amino acids 323–339 ($OVA_{323–339}$) epitopes were detected. Thus, late-stage demyelination was associated with the presence of MOG-specific autoreactive $CD4^+$ T cells in tamoxifen-treated DTA mice.

Since the presence of $MOG_{35–55}$-specific $CD4^+$ T cells in the peripheral lymphoid organs of young adult tamoxifen-treated DTA mice appeared to be below the level of functional detection owing to low precursor frequency in the absence of a strong stimulus such as priming with $MOG_{35–55}$ emulsified in complete Freund's adjuvant, we tested the activation and the proliferation of carboxyfluorescein succinimidyl ester (CFSE)-labeled naive $MOG_{35–55}$-specific T cell antigen receptor (TCR) transgenic T cells (2D2)[12] in the CNS and spleen 1 week after transfer into tamoxifen-treated DTA and control littermate (*ROSA26-eGFP-DTA*) recipient mice. The CFSE-labeled 2D2 $CD4^+$ T cells showed increased proliferation and production of proinflammatory cytokines interferon (IFN-γ) and interleukin (IL)-17 in both the CNS (Fig. 5a,b) and the spleens (Fig. 5c) of the tamoxifen-treated DTA mice. In addition, splenocytes collected from the tamoxifen-treated DTA mice showed increased proliferation and higher levels of the secreted proinflammatory T_H1 and T_H17 cytokines IFN-γ, granulocyte-macrophage colony stimulating factor (GM-CSF) and IL-17 upon *ex vivo* restimulation in the presence of $MOG_{35–55}$ peptide (Fig. 5d–g). These data indicate that activated $MOG_{35–55}$-specific T cells are present early in the CNS and spleens of the tamoxifen-treated DTA mice, raising the possibility that the CNS might be the primary initiation site of the autoimmune response against myelin observed in these animals later in life. This is the same anatomical location in which $CD4^+$ T cells expressing a TCR specific for another myelin peptide beside the disease-inducing myelin peptide (that is, spread epitope–specific $CD4^+$ T cells) are activated during relapsing-remitting EAE in SJL mice[13].

We also explored the possibility that the late-onset demyelination found in the CNS of tamoxifen-treated DTA mice was caused by oligodendrocyte loss due to tamoxifen-independent CreER^{T}-mediated recombination of the *ROSA26-eGPF-DTA* allele. This possibility was raised by our finding that modest levels of gene recombination occurred in the absence of tamoxifen treatment in *Plp1-CreER^{T};ROSA26-EYFP* reporter mice. Expression of the reporter protein YFP occurred in a small percentage of oligodendrocytes staining positive for CC-1 in all CNS areas of the untreated *Plp1-CreER^{T};ROSA26-EYFP* (reporter) mice at 52 weeks (Supplementary Fig. 2a). Therefore, we tested whether tamoxifen-independent recombination occurred in various CNS regions of the untreated reporter mice at younger ages. We found very few to no CC-1 and YFP double-positive cells at 13 weeks of age, whereas these cells were more numerous by 26 weeks of age. Likewise, there appeared to be a further increase in the number of CC-1 and YFP double-positive cells present in various CNS regions of untreated reporter mice with age, thereby showing a trend toward increased numbers of oligodendrocytes expressing YFP in most of these areas at 52 weeks (6–20%) compared to 26 weeks (6–14%) (Supplementary Fig. 2b).

Since a modest level of gene recombination appeared in the absence of tamoxifen treatment in the untreated reporter mice, we determined whether any neurological symptoms and myelin loss were present in untreated DTA mice as they aged. Although the untreated DTA mice appeared phenotypically normal up to 60 weeks of age (Supplementary Movie 2), they did show some myelin loss in most CNS areas at the age of 52 weeks via EM analysis (Supplementary Fig. 3a). Nevertheless, these mice did not display motor defects on the rotarod (Supplementary Fig. 4a) or substantial weight loss (Supplementary Fig. 4b) at time points when the tamoxifen-treated DTA mice were severely impaired. Moreover, these animals showed much less demyelination than the tamoxifen-treated DTA mice at 53 weeks after injection (Supplementary Fig. 3a). This finding was further supported by morphometric analysis of the corpus callosum, which showed that untreated DTA mice had ~30% fewer unmyelinated axons than tamoxifen-treated DTA mice (Supplementary Fig. 3b). In addition, tissue sections from both groups of mice showed myelinated axons with increased g-ratios, indicating thinner myelin, as compared to control (*ROSA26-eGFP-DTA*) mice (Supplementary Fig. 3c).

In contrast to that in the tamoxifen-treated DTA mice, CNS demyelination in untreated DTA mice was not associated with CD3^{+} T cell inflammation (Supplementary Fig. 5a) nor development of peripheral CD4^{+} T cell responses to MOG in lymphoid organs (Supplementary Fig. 5b). Furthermore, flow cytometric analysis of the CNS tissues and peripheral lymphoid organs showed equivalent numbers of various immune cell populations present in the spleen (Supplementary Fig. 5c), cervical lymph nodes (Supplementary Fig. 5d) and CNS (Supplementary Fig. 5e). Therefore, the late-stage demyelination in tamoxifen-treated DTA mice is specifically associated with CNS infiltration of activated CD4^{+} T cells and dendritic cells, as well as with the presence of peripheral MOG-specific autoreactive CD4^{+} T cells.

Adoptive transfer of DTA-derived MOG-specific T cells elicits CNS inflammation

Our finding of MOG-specific $CD4^+$ T cell responses in tamoxifen-treated DTA mice 40 weeks after injection raised the possibility that the late-onset demyelinating disease observed in these mice might be T cell mediated. To examine this possibility, we crossed the DTA model onto a *Rag1*$^{-/-}$ background[14]: *Rag1*$^{-/-}$ mice do not produce mature B or T cells. However, this approach was not successful because the tamoxifen-treated *Rag1*-deficient DTA mice did not recover from the acute demyelinating disease, indicating that T cells could act beneficially in CNS repair, as previously suggested[15–17]. Furthermore, we were not able to block T cells from entering the CNS[18] of the tamoxifen-treated DTA mice by repeated long-term injections of an anti-α4-integrin (VLA-4) rat monoclonal antibody (data not shown). The long-term exposure of these animals may have resulted in an immune response against the injected antibody. In line with this, it has been reported that a subset of MS patients treated with anti-VLA-4 monoclonal antibody (natalizumab) develop persistent neutralizing antibodies over the course of the treatment and show a loss of drug efficacy[19].

As an alternative approach, we determined the encephalitogenic potential of $MOG_{35–55}$-specific $CD4^+$ T cells in tamoxifen-treated DTA mice during the late-onset disease. Splenocytes were collected and cultured from these mice 40–52 weeks after injection or from control mice (*ROSA26-eGFP-DTA*) at the age of 57–69 weeks. Total splenocytes were activated *in vitro* in the presence of $MOG_{35–55}$, IL-12 and IL-2 for 3 d and 10^7 blast cells were transferred to *Rag1*$^{-/-}$ recipient mice[14]. In line with Figure 4e, blast cells (9.3 ± 1.56%) were present in the cultures from tamoxifen-treated DTA mice, whereas numbers of blast cells in cultures from control mice were negligible. The recipient mice were followed for disease, and the *Rag1*$^{-/-}$ mice that received $MOG_{35–55}$-activated DTA mouse cells showed a mild, but consistent and reproducible, EAE-like disease phenotype characterized by hindlimb weakness, mild ataxia and a hunched posture (Fig. 6a). Unlike with the use of $MOG_{35–55}$-specific T cells from donors primed with $MOG_{35–55}$ in complete Freund's adjuvant[20], we were able to transfer disease only to *Rag1*$^{-/-}$ mice, not to wild-type C57BL/J mice (Supplementary Fig. 6a,b). We consider this disease to be significant ($P < 0.001$ on days 24–39, two-way ANOVA with Bonferroni *post hoc* analysis) as we also found that $MOG_{35–55}$-specific TCR transgenic T cells purified from 2D2 mice and activated in T_H1- or T_H17-promoting conditions (Supplementary Fig. 6c) similarly could only mediate disease in *Rag1*$^{-/-}$ recipients. Additionally, while 2D2 $CD4^+$ T cells activated in the presence of T_H1- or T_H17-promoting conditions induced disease in *Rag1*$^{-/-}$ recipient mice, 2D2 $CD4^+$ T cells activated in the presence of T_H0-promoting conditions were not able to induce disease in *Rag1*$^{-/-}$ recipients (Supplementary Fig. 6d). On day 22 after cell transfer, the CNS and spleen were collected from the recipient mice. The number of total cells in the spleen and CNS of the recipients of cells from the tamoxifen-treated donor mice was significantly greater than in the recipients of cells from untreated control littermates (Fig. 6b,c). Histological analysis of brain and spinal cord sections from *Rag1*$^{-/-}$ mice revealed focal areas of T cell infiltration and increased microglia or macrophage activation by CD3 and IBA-1 immunostaining, respectively, which occurred mostly in the white matter–rich areas of the brainstem (Fig. 6d) and the corpus callosum (data not shown) of the mice inoculated with T cells derived from tamoxifen-treated DTA mice. Nevertheless, MBP staining looked normal (Fig. 6d), indicating that myelin may not be drastically disrupted in

these areas, despite the increased inflammation, consistent with the mild disease symptoms observed in the *Rag1*$^{-/-}$ mice inoculated with the DTA-derived cells.

A distinct adoptive transfer protocol in which fewer T cells (2×10^6) were transferred resulted in a milder neurological phenotype in the *Rag1*$^{-/-}$ recipients (data not shown). CNS samples from these animals were examined 42 d after transfer. EM analysis of brain and lower lumbar spinal cord from the recipient mice showed scattered focal areas of demyelination in the white matter of the cerebella and lower lumbar spinal cords of only mice inoculated with T cells derived from tamoxifen-treated DTA mice (Supplementary Fig. 7a). In these mice, the number of myelinated axons was reduced by around 30% compared to that in mice inoculated with T cells from control mice (Supplementary Fig. 7b).

The above findings suggest that DTA-derived $MOG_{35–55}$ activated splenic $CD4^+$ T cells are able to enter the CNS and induce a mild demyelinating disease following adoptive transfer into *Rag1*$^{-/-}$ recipient mice. Therefore, we tested whether $MOG_{35–55}$-specific immune tolerance using the intravenous (i.v.) infusion of $MOG_{35–55}$-coupled poly(lactic-co-glycolic acid) (PLG) nanoparticles[21] could inhibit the ability of DTA-derived $MOG_{35–55}$ activated splenic $CD4^+$ T cells to induce disease in *Rag1*$^{-/-}$ recipient mice. The treatment of DTA-derived cell recipient mice with $MOG_{35–55}$-coupled PLG nanoparticles on the day of $MOG_{35–55}$ blast cell transfer significantly inhibited disease severity as compared to that in DTA-derived cell recipient mice treated with $OVA_{323–339}$-coupled PLG particles (Fig. 7a). On day 30 after disease induction, the number and phenotype of $CD4^+$ T cells present in the CNS and spleen was assessed via flow cytometric analysis. Treatment of DTA-derived cell recipient mice with $MOG_{35–55}$-PLG inhibited the infiltration of total $CD4^+$, IFN-γ^+CD4^+, IL-17^+CD4^+, and $Ki67^+CD4^+$ T cells into the CNS, as compared to that in DTA-derived cell recipient mice receiving $OVA_{323–339}$-PLG treatment (Fig. 7b,c and Supplementary Fig. 8a–c). In contrast, there was a significantly higher number of total $CD4^+$ T cells in the spleen of the $MOG_{35–55}$-PLG-treated DTA-derived cell recipient mice, as compared to that in $OVA_{323–339}$-PLG treated DTA-derived cell recipient mice, but no statistical difference in the number of IFN-γ^+CD4^+, IL-17^+CD4^+, and $Ki67^+CD4^+$ T cells between the $MOG_{35–55}$-PLG- and $OVA_{323–339}$-PLG-treated DTA-derived cell recipient mice (Fig. 7d,e and Supplementary Fig. 8d–f). These findings suggest that the $MOG_{35–55}$-specific $CD4^+$ T cells present in the late-stage tamoxifen-treated DTA mice display encephalitogenic potential.

$MOG_{35–55}$ specific tolerance inhibits late-onset disease

To further explore the encephalitogenic potential of the MOG-specific $CD4^+$ T cells in tamoxifen-treated DTA mice, we determined whether the induction of $MOG_{35–55}$-specific tolerance could block the progression of late-onset disease symptoms. Tamoxifen-treated DTA mice received $MOG_{35–55}$- or $OVA_{323–339}$-coupled PLG nanoparticles 32 weeks after injection via i.v. injection. Treatment with $MOG_{35–55}$-PLG inhibited disease progression in the tamoxifen-treated DTA mice as compared to that in tamoxifen-treated DTA mice treated with $OVA_{323–339}$-PLG, as assessed via motor function defects (Fig. 8a) and weight loss (Fig. 8b). $MOG_{35–55}$-specific tolerance also decreased $CD4^+$ T cell infiltration, proliferation and production of the proinflammatory cytokine IFN-γ in the CNS (Fig. 8c and Supplementary Fig. 9a–g), but not the spleens of the DTA mice (Fig. 8d and Supplementary Fig. 9h–m).

When isolated splenocytes from the $MOG_{35–55}$-tolerized tamoxifen-treated DTA mice were cultured *in vitro* in the presence of the $MOG_{35–55}$ peptide, they secreted lower levels of the proinflammatory cytokine IFN-γ (Fig. 8e), did not produce appreciable amounts of IL-17 (Fig. 8f), and showed decreased proliferation (Fig. 8g), consistent with the expected tolerance to the $MOG_{35–55}$ peptide. Overall, the data strongly favor the conclusion that the late-onset disease in tamoxifen-treated DTA mice is mediated by activated $CD4^+$ MOG-specific T cells, which arise as a result of the oligodendrocyte ablation in early life.

DISCUSSION

The evidence presented here strongly suggests that induction of extensive oligodendrocyte loss in young adult DTA mice is sufficient to activate $CD4^+$ T cell–mediated immune responses against myelin that lead to a severe, late-onset demyelinating disease. Although oligodendrocyte loss in tamoxifen-treated DTA mice did not activate the adaptive immune system at the peak of acute disease (5 weeks after injection), substantial CNS infiltration of activated $CD4^+$ T cells occurred during the remyelination stages (at 10 weeks after injection). Furthermore, all tamoxifen-treated DTA mice in this study developed a fatal, secondary demyelinating disease starting approximately 40 weeks after injection. At this late-onset disease time point, focal inflammatory demyelinating lesions were found in various white matter–rich CNS areas of the tamoxifen-treated DTA mice. These focal lesions appeared to progress, as extensive myelin loss was observed throughout the CNS 1 year after injection. These late changes were associated with infiltration of activated $CD4^+$ T cells and dendritic cells into the CNS. We also found that $MOG_{35–55}$-specific T cells were present in the peripheral lymphoid organs of tamoxifen-treated DTA mice at the time of CNS infiltration, which indicates an ongoing immune response against myelin during the late-onset disease.

In support of the conclusion that myelin peptide–specific $CD4^+$ T cells become reactivated at later time points after oligodendrocyte ablation, we found activated $CD4^+$ T cells to be already present in the CNS of the tamoxifen-treated DTA mice much earlier as assessed via flow cytometric analysis 10 weeks after injection. Additionally, in cell tracking experiments, a higher number of transferred CFSE-labeled $MOG_{35–55}$-specific 2D2 $CD4^+$ T cells were present in the CNS of the DTA mice during the recovery period after ablation, and these T cells were more proliferative and a greater number were either IFN-γ^+ or IL-17^+ when compared to those in control littermate recipients. Taken together, these data indicate that the CNS might be the primary initiation site of the autoimmune response against myelin observed in these animals during the late-onset disease.

Like progressive MS[22], the late-onset demyelinating disease in the tamoxifen-treated DTA mice is also associated with axonal loss in the CNS. Therefore, this mouse model is ideal for studying the mechanisms of neuronal degeneration in adult-onset demyelinating diseases like MS, as well as for validating new therapeutic treatments that could promote remyelination and neuroprotection in the CNS.

Late-onset disease was not associated with appreciable oligodendrocyte loss in most areas of the CNS. We did, however, detect a low level of tamoxifen-independent recombination in the

CreER^T driver line (*Plp1-CreER*^{T}) used in the DTA model (Supplementary Fig. 2). Nevertheless, demyelination in untreated DTA mice was mild and the mice showed no neurological symptoms. Moreover, this tamoxifen-independent demyelination was not associated with myelin-specific T cell responses or inflammation in the CNS. This finding supports the hypothesis that induction of extensive oligodendrocyte loss is required for the activation of the MOG-specific T cell responses detected in tamoxifen-treated DTA mice during the secondary, late-onset demyelinating disease. The association between severe demyelination in tamoxifen-treated DTA mice and the presence of inflammatory $CD4^+$ T cells and dendritic cells in the CNS suggest that the late-onset demyelination is mediated by MOG-specific T cells found in these animals. This possibility is further supported by the proliferative and proinflammatory T_H1 (IFN-γ) and T_H17 (IL-17) responses by $MOG_{35–55}$-specific $CD4^+$ T cells present in tamoxifen-treated DTA mice and by the ability of these cells to consistently induce EAE-like neurological symptoms that correlated with active inflammatory lesions in the CNS white matter when inoculated into naive *Rag1*$^{-/-}$ mice. The absence of a B-cell response in the *Rag1*$^{-/-}$ recipient mice[14] might explain why more severe clinical symptoms were not observed. Lastly, an autoimmune basis for the late-onset disease in DTA mice is strongly supported by our data showing amelioration of the late-onset disease symptoms in tamoxifen-treated DTA mice that were tolerized specifically to the $MOG_{35–55}$ peptide.

It is intriguing that although autoimmune responses against myelin peptides have been detected in mice after they were administered the demyelinating neurotoxin cuprizone for 4 weeks and switched to normal diet for 2 weeks (ref. 23), secondary CNS demyelination has not been detected in the cuprizone mouse model after long-term survival[24]. Also, we have not found evidence of late-onset CNS demyelination and T cell infiltration in cuprizone-fed C57BL/6J mice surviving as long as 10 months after recovering from oligodendrocyte loss and demyelination (M.T. and B.P. unpublished data). One possible explanation for these differences is simply that demyelination is more widespread in the DTA model, generating more myelin antigen, than in mice treated with cuprizone, which primarily affects the corpus callosum and superior cerebellar peduncle[25]. Alternatively, or additionally, cuprizone might have a direct immunosuppressant effect. In support of this possibility, it has also been shown that cuprizone inhibits the development of EAE as well as graft-versus-host disease, and that these effects correlate with alterations to peripheral T cell responses[26].

Our evidence seems to contradict the study of oligodendrocyte ablation in the oligodendrocyte-expressed diphtheria toxin receptor (oDTR) genetic mouse model, in which oligodendrocyte death does not induce an adaptive immune response against myelin even under conditions that favor autoimmunity[27]. Induction of oligodendrocyte death and CNS demyelination in the oDTR model are achieved by direct administration of diphtheria toxin; this leads to neurode-generation that results in a severe phenotype and premature death. Therefore, detection of secondary anti-CNS immunity in the oDTR model might be precluded by the early death of the mice. Also, several genetic mouse models of inducible oligodendrocyte death have been described, all of which exhibit severe phenotypes and early death, which precludes the ability to track the mice over an extended time course, as was done in the present model system[28–32]. Nevertheless, no T cell infiltration of the CNS has been reported in any of these models, which further suggests that long-term survival after

oligodendrocyte death is crucial to the development of autoimmunity and late-onset disease in the DTA model. Thus, development of CNS autoimmunity after oligodendrocyte loss could be a slow process. This delay might explain the difficulty in observing a correlation between oligodendrocyte loss, whether induced by viral cytotoxicity or other environmental factors, and a myelin immune response in patients with MS[5]. In line with this idea, it has been shown recently that nascent MS lesions with oligodendrocyte loss, in the absence of the adaptive immune infiltrates, occurred in a patient who tested positive for the *Clostridium perfringens* type B, indicating that MS might be triggered by an agent cytotoxic to oligodendrocytes[33]. Both type B and D strains of *C. perfringens* cause a severe demyelinating disease in ruminant animals that is similar to human MS by producing ε-toxin, which specifically targets and kills mature oligodendrocytes in the CNS[34].

Notably, focal oligodendrocyte death in the CNS induced by lentivirus-mediated expression of caspase 9 leads to the infiltration of $CD3^+$ T cells into demyelinated areas[35], which is similar to the response in the DTA mouse model, although the presence of myelin-specific immune responses was not investigated in the lentivirus model. Furthermore, T cell infiltration has been detected in the CNS of mice carrying genetic defects that result in oligodendrocyte abnormalities, such as *Pex5* conditional knockout mice[36], *Plp1*-overexpressing mice[37], and galactosylceramidase-deficient twitcher mice, a murine model of the severe demyelinating Krabbe disease[38–40]. Therefore, CNS immune responses secondary to oligodendrocyte abnormalities may be more common than previously appreciated and, as demonstrated by the late-onset DTA model, may be of clinical significance. Nevertheless, several studies have unequivocally shown that MS susceptibility is mostly associated with genes that are linked to the immune system[41,42], indicating that a permissive immune system is also required for the primary oligodendrocyte damage to lead to MS pathogenesis.

Overall, our data show that oligodendrocyte death in young animals, which occurs in the absence of blood-brain barrier breakdown[8], can induce late-onset CNS autoimmunity. This evidence supports the ‘inside-out’ hypothesis: certain forms of MS may be caused by primary oligodendrocyte loss or myelin damage that secondarily leads to activation of the permissive adaptive immune system and CNS inflammation. Therefore, we believe that the DTA mouse model is uniquely suited to elucidating the initiation of CNS autoimmunity, which is not well understood. This mouse model also offers the opportunity to screen new therapeutic approaches to prevent activation of the adaptive immune system and thereby protect the CNS from immune-mediated inflammatory damage. Moreover, the late-onset DTA disorder, which is characterized by widespread demyelination, axonal loss and persistent clinical deterioration, is reminiscent of the progressive phase of MS, suggesting that the DTA model might provide critical insight into the pathogenesis of late-stage, chronic MS.

ONLINE METHODS

Mice

The *ROSA26-eGFP-DTA* (ref. 43), the *ROSA26-stop-EYFP* (ref. 44), the *Rag1* knockout[14] (*Rag1*$^{-/-}$) and the 2D2 transgenic[12] mice were purchased from the Jackson Laboratory. The *ROSA26-eGFP-DTA* and the *ROSA26-stop-YFP* mice were bred to the *Plp1-CreER*^{T}

transgenic mice[9] to generate the *Plp1-CreER^T;ROSA26-eGFP-DTA* (DTA) and *Plp1-CreER^T;ROSA26-stop-EYFP* (reporter) mice, as previously described[8]. All mouse studies were conducted in compliance with The University of Chicago's and Northwestern University's Animal Care and Use Committee (IACUC) guidelines.

Tamoxifen injections

Plp1-CreER^T;ROSA26-eGFP-DTA mice 5–7 weeks old were injected intraperitoneally with 0.8 mg of 4-hydroxytamoxifen (H-6278, Sigma) per day, either for 5 consecutive days (males) or 3 consecutive days (females). We refer to these as tamoxifen-treated DTA mice. The *Plp1-CreER^T;ROSA26-eGFP-DTA* mice that did not receive tamoxifen injections are referred to as untreated DTA mice. *ROSA26-eGFP-DTA* littermates were used as control mice in all studies involving the tamoxifen-treated DTA or the untreated DTA mice.

Flow cytometry

Splenic and CNS leukocytes were isolated from the brain and spinal cords of individual mice perfused with 20 mL of PBS. Single-cell suspensions were prepared as previously described[13]. Flow cytometry was performed on cells from individual animals. Cells were stained using a combination of antibodies to analyze T cell and APC populations: anti-CD45 (clone 30-F11, BD Bioscience cat. no. 47–0451), anti-CD3 (clone 145-2C11; BD Bioscience cat. no.553067), anti-CD4 (clone RM4–5; eBioscience cat. no. 25–0042), anti-CD8α (clone 53-6.7; eBioscience cat. no. 17–0081), anti-CD25 (clone PC61; eBioscience cat. no. 12–0251), anti-CD44 (clone IM7; eBioscience cat. no. 17–0441), anti-IFN-γ (clone XMG1.2; eBioscience cat. no. 11–7311), anti-IL-17 (clone eBio17B7; eBioscience cat. no. 12–7177), anti-Ki67 (clone SolA15; eBioscience cat. no. 48–5698), anti-CD11b (clone M1/70; eBioscience cat. no. 25–0112), anti-CD11c (clone HL3; BD Bioscience cat. no. 561045), anti-CD19 (clone ID3; eBioscience cat. no. 48–0193), anti-MHC II (I-A^b) (clone 25-9-17; BD Bioscience cat. no. 553552), anti-B7 (anti-CD80)-APC (clone 16–10A1; BD Bioscience cat. no. 560016) and anti-CD86 (clone GL1; BD Bioscience cat. no. 561964). Viable cells (1×10^6 cells per tube) were analyzed per individual sample using a BD Canto II cytometer (Becton Dickinson), and the data were analyzed using BD FACSDiva version 6.1 software (BD Bioscience).

In vitro splenocyte activation and adoptive transfer of $MOG_{35–55}$-specific T cells to naive *Rag1$^{-/-}$* mice

Total splenocytes were collected from age-matched control littermate (*ROSA26-eGFP-DTA*) mice or tamoxifen-treated DTA mice, and cells were activated in the presence of anti-CD3 (1 μg/ml), $OVA_{323–339}$, $PLP_{139–151}$, $PLP_{178–191}$, $MBP_{84–104}$, $MOG_{35–55}$ or whole recombinant rat MOG protein (10 μg/ml). The cells were cultured at 1×10^6 cells per well in a 96-well plate in HL-1 medium. The cultures were pulsed with tritiated thymidine (1 μCi) at 24 h and cultures were harvested 72 h after culture to determine cellular proliferation. Tritiated thymidine incorporation was detected using a Topcount Microplate Scintillation Counter. For the $MOG_{35–55}$-specific T cell transfer experiments, spleens were collected from age-matched control littermate or DTA mice during the late-onset disease—for example, 40 weeks after injection. Total splenocytes were activated in the presence of $MOG_{35–55}$ peptide (20 μg/ml) plus IL-12 (10 ng/ml) and IL-2 (100 U/ml) at a cell density of 10^7 cells/ml in

HL-1 medium in a T76 flask. After 3 d of culture, the cells were harvested and enumerated via a hemocytometer using trypan blue. A total of 10^7 blast cells from the tamoxifen-treated DTA mice cultures were transferred into each recipient *Rag1*$^{-/-}$ mouse on a C57BL/6 background (Jackson Laboratory; Bar Harbor, ME) via i.v. injection. Alternatively, a milder model of disease was induced via activation of splenocytes in the presence of $MOG_{35–55}$ peptide (20 μg/ml) plus IL-12 (10 ng/ml) in the absence of IL-2 and fewer blast cells (2×10^6) were transferred into each *Rag1*$^{-/-}$ mice. Since the control littermate cells did not have any blast cells, what would be an equivalent number based on culture input cells to the input cells for the tamoxifen-treated DTA mice cells were transferred into *Rag1*$^{-/-}$ recipient mice. All recipient mice also received pertussis toxin (200 ng per injection) via i.p. injection on days 0 and 2 after cell transfer. Individual animals were observed at the indicated time points and clinical scores assessed in a blinded fashion on a 0–5 scale: 0, no abnormality; 1, limp tail; 2, limp tail and hind limb weakness; 3, hind limb paralysis; 4, hind limb paralysis and forelimb weakness; and 5, moribund. The data are reported as the mean daily clinical score.

CFSE-labeled $MOG_{35–55}$-specific TCR transgenic (2D2) T cell transfer to young adult DTA mice

Naive $CD4^+$ T cells were purified from the spleens of $MOG_{35–55}$-specific TCR transgenic (2D2) mice 6–10 weeks old via AutoMax separation (Miltenyi) using the untouched $CD4^+$ T cells sort followed by $CD62L^+$ sorting, and the cells were found to be ~95–98% $CD3^+CD4^+$. The naive $CD4^+$ T cells were labeled with CFSE (4 μM), and 5×10^6 cells were transferred via i.v. injection into control and tamoxifen-treated DTA mice. On day 7 after CFSE-labeled $CD4^+$ T cells transfer, the recipient mice were anesthetized and perfused, and spleen and CNS samples were collected for flow cytometry.

$MOG_{35–55}$-PLG-induced tolerance

PLG-PEMA nanoparticles were prepared using a single emulsion solvent evaporation method[21]. Peptide antigens were attached to the surface of 500-nm carboxylated PLG particles using ECDI (1-ethyl-3-(3′-dimethylaminopropyl)carbodiimide; EMD Chemicals, Inc., Gibbstown, NJ) with 0.08 mg of peptide in the presence of 0.32 mg ECDI per mg of PLG nanoparticles. Animals received intravenous injections of approximately 9×10^9 nanoparticles comprising 10–15 μg of peptide, depending on the sequence used in the coupling reaction. Carboxylated 500-nm polystyrene beads were purchased from Polysciences (Warrington, PA). Peptide antigens were attached to particles using ECDI according to manufacturer's instructions, in the same process and concentration as for the PLG nanoparticles. Individual animals were observed at the indicated time points and clinical scores assessed in a blinded fashion on a 0–6 scale: 0, no abnormality; 1, wobbly gait; 2, mild ataxia and tremor; 3, severe ataxia and tremor; 4, ataxia and tremor with hindlimb dragging; 5, ataxia and tremor with stiff gait (the mouse falls over); 6, lateral recumbent. The data are reported as the mean daily clinical score.

Histology, immunohistochemistry and electron microscopy analysis

Histology, immunohistochemistry and electron microscopy (EM) analysis were performed as previously described[45] with slight modifications. Mice were perfused through the heart with 4% paraformaldehyde in 0.1 M phosphate buffer (pH 7.3). Half of the brains and

cervical spinal cords were processed for immunohistochemistry and the other half for EM analysis. The following primary antibodies were used for immunohistochemistry: mouse monoclonal antibodies against CC-1 (1:50; Calbiochem, cat. no. OP80), MBP (1:1,000; BioLegend, cat. no. SMI99) and SMI31 (anti-phosphorylated neurofilament H, 1:1,000; BioLegend, cat. no. SMI-31R); rat monoclonal antibodies against CD3 (1:500; 17A2, Santa Cruz Biotechnology, cat. no. sc-18843) and CD11b (1:50; ABD Serotec, cat. no. NC9460003); and rabbit polyclonal antibodies against CD3 (1:100; Abcam, cat. no. AB5690), GFP (1:500; Invitrogen, cat. no. A-21311), MBP (1:1,000; Abcam, cat. no. ab40390) and IBA-1 (1:1,000; Wako Pure Chemical Industries, cat. no. 019–19741). Immunofluorescence images were collected on a Leica SP5 II AOBS tandem scanner spectral confocal system on a DMI6000 microscope and controlled by LASAF software (version 2.7.3.9723). Tiled capture of *z*-stacks was automatically collected and images merged using the stage-scanning feature of the microscope and LASAF software. Four channels were collected at each location using sequential excitation (405, 488, 561, 633 nm; emission: 412–452, 495–537, 578–631 and 654–755 nm pass bands) on either photomultiplier or HyD hybrid detectors. Objectives used were ×20, NA 0.7 dry and ×63, NA 1.40 oil (Leica). EM images were collected with a FEI Tecnai F30 Supertwin electron microscope operated at 300 kV using the Gatan Ultrascan 4K camera controlled by the Gatan DigitalMicrograph software. For histology of the *Rag1*$^{-/-}$ recipient mouse tissues, we isolated half of the fresh brains and the lower segment of the lumbar spinal cords and fixed them by immersion in 4% paraformaldehyde (pH 7.3) overnight at 4 °C. Sixteen sagittal brain cryosections (10 μm thick) were collected sequentially every 50 μm for immunohistochemistry.

Brainstem EM counts

We randomly collected 10–30 non-overlapping EM images (×2,900 magnification) of the brainstem gray matter area at the level of the pons from each *Rag1*$^{-/-}$ naive recipient mouse 42 d after transfer to calculate the mean density of myelinated axons in this area.

Axonal counts

Four to seven non-overlapping EM images (×2,900 or ×3,900 magnification) of the corpus callosum at the level of the fornix were collected from each mouse and used to count the percentage of unmyelinated axons and calculate the g-ratios (axonal diameter/fiber diameter) as previously described[46] using NIH ImageJ software. g-ratios were calculated from 120 axons per genotype. Only axons with a diameter ≥0.30 μm were included in the analysis[46]. For the axonal counts, we collected three non-overlapping images (×40 magnification) of the ventrolateral white matter on toluidine blue–stained cross sections of the spinal cord at the cervical enlargement and four non-overlapping images of the optic nerve (×100 magnification) to calculate the mean axonal density in each mouse ($n = 3$ mice per genotype) using the NIH ImageJ software. The total number of axons was calculated by multiplying the mean axonal density by the total surface area of the corresponding toluidine blue–stained section of each area measured by ImageJ as previously described[8].

Rotarod testing

We measured the motor coordination and balance of untreated or tamoxifen-treated *Plp1-CreER^T;ROSA26-eGFP-DTA* (DTA) male mice and *ROSA26-eGFP-DTA* littermate control male mice on a rotarod (Stoelting Co.). The mice were trained to maintain themselves on the rotarod at a constant speed (5 r.p.m.), and then were tested once a week (4 trial sessions). During the 5-min trial sessions, we monitored the time (latency) that each mouse spent on the rotating rod in accelerating speed mode (5–45 r.p.m.).

Statistical analysis

Data from all experimental mice and controls were compared using the unpaired one-tailed or two-tailed Student's *t*-test, one-way ANOVA followed by Tukey's *post hoc* analysis test (for multiple comparisons versus control), or two-way ANOVA with a Bonferroni post-test. No statistical methods were used to predetermine samples sizes, but our samples were chosen on the basis of the availability of mice given the constraints of the individual experiments. Data distribution was assumed to be normal, but this was not formally tested. The mice in specific disease course experiments were randomized and coded, such that the mice were scored in a double-blinded manner. The α level was set at 0.05 and differences were considered to be statistically significant when $P < \alpha$.

A **Supplementary Methods checklist** is available.

Supplementary Material

Refer to Web version on PubMed Central for supplementary material.

Acknowledgments

We thank E. Liu, A. Solanki, A.X. Tang and S. Labak for technical assistance, G. Wright for assistance with the morphometric analysis of the EM images using the ImageJ software and V. Bindokas from the University of Chicago Integrated Light Microscopy Core Facility for help with image acquisition and image processing. The work was supported by awards from the Myelin Repair Foundation and the National Multiple Sclerosis Society (RG 4952-A-5) to B.P. and S.D.M.

References

1. Nylander A, Hafler DA. Multiple sclerosis. J. Clin. Invest. 2012; 122:1180–1188. [PubMed: 22466660]
2. Nakahara J, Aiso S, Suzuki N. Autoimmune versus oligodendrogliopathy: the pathogenesis of multiple sclerosis. Arch. Immunol. Ther. Exp. (Warsz.). 2010; 58:325–333. [PubMed: 20676785]
3. McFarland HF, Martin R. Multiple sclerosis: a complicated picture of autoimmunity. Nat. Immunol. 2007; 8:913–919. [PubMed: 17712344]
4. Stys PK, Zamponi GW, van Minnen J, Geurts JJ. Will the real multiple sclerosis please stand up? Nat. Rev. Neurosci. 2012; 13:507–514. [PubMed: 22714021]
5. Barnett MH, Prineas JW. Relapsing and remitting multiple sclerosis: pathology of the newly forming lesion. Ann. Neurol. 2004; 55:458–468. [PubMed: 15048884]
6. Henderson AP, Barnett MH, Parratt JD, Prineas JW. Multiple sclerosis: distribution of inflammatory cells in newly forming lesions. Ann. Neurol. 2009; 66:739–753. [PubMed: 20035511]
7. Rodriguez M, Scheithauer B. Ultrastructure of multiple sclerosis. Ultrastruct. Pathol. 1994; 18:3–13. [PubMed: 8191643]

8. Traka M, et al. A genetic mouse model of adult-onset, pervasive central nervous system demyelination with robust remyelination. Brain. 2010; 133:3017–3029. [PubMed: 20851998]
9. Doerflinger NH, Macklin WB, Popko B. Inducible site-specific recombination in myelinating cells. Genesis. 2003; 35:63–72. [PubMed: 12481300]
10. Feil R, et al. Ligand-activated site-specific recombination in mice. Proc. Natl. Acad. Sci. USA. 1996; 93:10887–10890. [PubMed: 8855277]
11. Bailey SL, Schreiner B, McMahon EJ, Miller SD. CNS myeloid DCs presenting endogenous myelin peptides 'preferentially' polarize $CD4^+$ T_H-17 cells in relapsing EAE. Nat. Immunol. 2007; 8:172–180. [PubMed: 17206145]
12. Bettelli E, Baeten D, Jäger A, Sobel RA, Kuchroo VK. Myelin oligodendrocyte glycoprotein-specific T and B cells cooperate to induce a Devic-like disease in mice. J. Clin. Invest. 2006; 116:2393–2402. [PubMed: 16955141]
13. McMahon EJ, Bailey SL, Castenada CV, Waldner H, Miller SD. Epitope spreading initiates in the CNS in two mouse models of multiple sclerosis. Nat. Med. 2005; 11:335–339. [PubMed: 15735651]
14. Mombaerts P, et al. RAG-1-deficient mice have no mature B and T lymphocytes. Cell. 1992; 68:869–877. [PubMed: 1547488]
15. Butovsky O, et al. Microglia activated by IL-4 or IFN-gamma differentially induce neurogenesis and oligodendrogenesis from adult stem/progenitor cells. Mol. Cell. Neurosci. 2006; 31:149–160. [PubMed: 16297637]
16. Pusic AD, Pusic KM, Clayton BL, Kraig RP. IFNγ-stimulated dendritic cell exosomes as a potential therapeutic for remyelination. J. Neuroimmunol. 2014; 266:12–23. [PubMed: 24275061]
17. Schwartz M, Raposo C. Protective autoimmunity: a unifying model for the immune network involved in CNS repair. Neuroscientist. 2014; 20:343–358. [PubMed: 24395337]
18. Yednock TA, et al. Prevention of experimental autoimmune encephalomyelitis by antibodies against α4β1 integrin. Nature. 1992; 356:63–66. [PubMed: 1538783]
19. Polman CH, et al. A randomized, placebo-controlled trial of natalizumab for relapsing multiple sclerosis. N. Engl. J. Med. 2006; 354:899–910. [PubMed: 16510744]
20. Podojil JR, et al. B7-H4Ig inhibits mouse and human T-cell function and treats EAE via IL-10/Treg-dependent mechanisms. J. Autoimmun. 2013; 44:71–81. [PubMed: 23683881]
21. Hunter Z, et al. A biodegradable nanoparticle platform for the induction of antigen-specific immune tolerance for treatment of autoimmune disease. ACS Nano. 2014; 8:2148–2160. [PubMed: 24559284]
22. Bjartmar C, Wujek JR, Trapp BD. Axonal loss in the pathology of MS: consequences for understanding the progressive phase of the disease. J. Neurol. Sci. 2003; 206:165–171. [PubMed: 12559505]
23. Maña P, et al. Demyelination caused by the copper chelator cuprizone halts T cell mediated autoimmune neuroinflammation. J. Neuroimmunol. 2009; 210:13–21. [PubMed: 19344958]
24. Manrique-Hoyos N, et al. Late motor decline after accomplished remyelination: impact for progressive multiple sclerosis. Ann. Neurol. 2012; 71:227–244. [PubMed: 22367995]
25. Blakemore WF. Demyelination of the superior cerebellar peduncle in the mouse induced by cuprizone. J. Neurol. Sci. 1973; 20:63–72. [PubMed: 4744511]
26. Emerson MR, Biswas S, LeVine SM. Cuprizone and piperonyl butoxide, proposed inhibitors of T-cell function, attenuate experimental allergic encephalomyelitis in SJL mice. J. Neuroimmunol. 2001; 119:205–213. [PubMed: 11585623]
27. Locatelli G, et al. Primary oligodendrocyte death does not elicit anti-CNS immunity. Nat. Neurosci. 2012; 15:543–550. [PubMed: 22366759]
28. Buch T, et al. A Cre-inducible diphtheria toxin receptor mediates cell lineage ablation after toxin administration. Nat. Methods. 2005; 2:419–426. [PubMed: 15908920]
29. Ghosh A, et al. Targeted ablation of oligodendrocytes triggers axonal damage. PLoS One. 2011; 6:e22735. [PubMed: 21818378]

30. Pohl HB, et al. Genetically induced adult oligodendrocyte cell death is associated with poor myelin clearance, reduced remyelination, and axonal damage. J. Neurosci. 2011; 31:1069–1080. [PubMed: 21248132]
31. Oluich LJ, et al. Targeted ablation of oligodendrocytes induces axonal pathology independent of overt demyelination. J. Neurosci. 2012; 32:8317–8330. [PubMed: 22699912]
32. Gritsch S, et al. Oligodendrocyte ablation triggers central pain independently of innate or adaptive immune responses in mice. Nat. Commun. 2014; 5:5472. [PubMed: 25434649]
33. Rumah KR, Linden J, Fischetti VA, Vartanian T. Isolation of *Clostridium perfringens* type B in an individual at first clinical presentation of multiple sclerosis provides clues for environmental triggers of the disease. PLoS One. 2013; 8:e76359. [PubMed: 24146858]
34. Linden JR, et al. *Clostridium perfringens* epsilon toxin causes selective death of mature oligodendrocytes and central nervous system demyelination. MBio. 2015; 6:e02513. [PubMed: 26081637]
35. Caprariello AV, Mangla S, Miller RH, Selkirk SM. Apoptosis of oligodendrocytes in the central nervous system results in rapid focal demyelination. Ann. Neurol. 2012; 72:395–405. [PubMed: 23034912]
36. Kassmann CM, et al. Axonal loss and neuroinflammation caused by peroxisome-deficient oligodendrocytes. Nat. Genet. 2007; 39:969–976. [PubMed: 17643102]
37. Ip CW, et al. Immune cells contribute to myelin degeneration and axonopathic changes in mice overexpressing proteolipid protein in oligodendrocytes. J. Neurosci. 2006; 26:8206–8216. [PubMed: 16885234]
38. Ohno M, Komiyama A, Martin PM, Suzuki K. MHC class II antigen expression and T-cell infiltration in the demyelinating CNS and PNS of the twitcher mouse. Brain Res. 1993; 625:186–196. [PubMed: 8275302]
39. Suzuki K. Twenty five years of the “psychosine hypothesis”: a personal perspective of its history and present status. Neurochem. Res. 1998; 23:251–259. [PubMed: 9482237]
40. Suzuki K. Globoid cell leukodystrophy (Krabbe’s disease): update. J. Child Neurol. 2003; 18:595–603. [PubMed: 14572137]
41. Hafler DA, et al. Risk alleles for multiple sclerosis identified by a genomewide study. N. Engl. J. Med. 2007; 357:851–862. [PubMed: 17660530]
42. Sawcer S, et al. Genetic risk and a primary role for cell-mediated immune mechanisms in multiple sclerosis. Nature. 2011; 476:214–219. [PubMed: 21833088]
43. Ivanova A, et al. In vivo genetic ablation by Cre-mediated expression of diphtheria toxin fragment A. Genesis. 2005; 43:129–135. [PubMed: 16267821]
44. Srinivas S, et al. Cre reporter strains produced by targeted insertion of EYFP and ECFP into the ROSA26 locus. BMC Dev. Biol. 2001; 1:4. [PubMed: 11299042]
45. Traka M, et al. Nur7 is a nonsense mutation in the mouse aspartoacylase gene that causes spongy degeneration of the CNS. J. Neurosci. 2008; 28:11537–11549. [PubMed: 18987190]
46. Shen S, et al. Age-dependent epigenetic control of differentiation inhibitors is critical for remyelination efficiency. Nat. Neurosci. 2008; 11:1024–1034. [PubMed: 19160500]

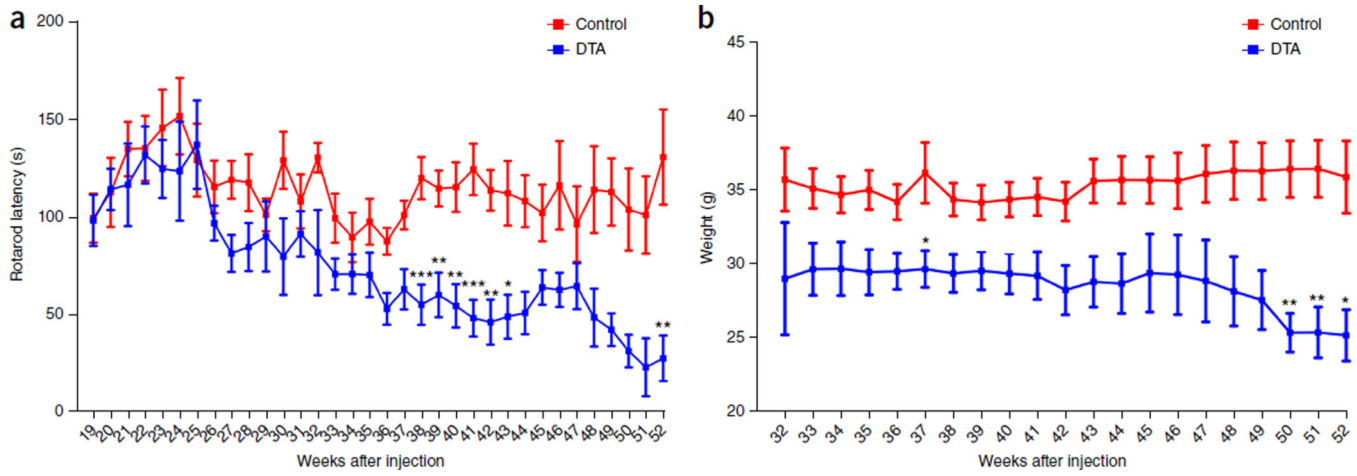

Figure 1.

DTA mice develop a severe late-onset clinical phenotype. (**a**) Tamoxifen-treated *Plp1-CreER^{T};ROSA26-eGFP-DTA* mice displayed significantly reduced latency on the rotarod starting around 38 weeks after injection as compared to the control littermate (*ROSA26-eGFP-DTA*) mice. Control mice: 19–32 weeks, $n = 5$; 33 and 46–51 weeks, $n = 9$; 34, 35 and 43–45 weeks, $n = 11$; 36, 41 and 42 weeks, $n = 14$; 37–40 weeks, $n = 15$; 52 weeks, $n = 7$. DTA mice: 19–32 weeks, $n = 4$; 33 and 42 weeks, $n = 10$; 34 weeks, $n = 12$; 35 and 41 weeks, $n = 11$; 36–39 weeks, $n = 15$; 40 weeks, $n = 14$; 43 weeks, $n = 9$; 44 weeks, $n = 7$; 45–50 weeks, $n = 5$; 51–52 weeks, $n = 3$. Significance between control and DTA mice: 38 weeks, $P = 0.0005$; 39 weeks, $P = 0.0094$; 40 weeks, $P = 0.0024$; 41 weeks, $P = 0.0002$; 42 weeks, $P = 0.0025$; 43 weeks, $P = 0.0207$; 52 weeks, $P = 0.0095$. (**b**) Concurrently with the late-onset disease, the tamoxifen-treated DTA mice showed significant weight loss as compared to control littermate mice. Control mice: 32 weeks, $n = 5$; 33 weeks, $n = 10$; 34–35 and 43–45 weeks, $n = 11$; 36, 41 and 42 weeks, $n = 14$; 37–40 weeks, $n = 15$; 46–51 weeks, $n = 9$; 52 weeks, $n = 7$. DTA mice: 32 weeks, $n = 4$; 33–34 weeks, $n = 10$; 35 and 41 weeks, $n = 12$; 36–39 weeks, $n = 16$; 40 weeks, $n = 15$; 42 weeks, $n = 11$; 43 weeks, $n = 9$; 44 weeks, $n = 8$; 45–49 weeks, $n = 6$; 50–52 weeks, $n = 5$. Significance between control and DTA mice: 37 weeks, $P = 0.021$; 50 weeks, $P = 0.0063$; 51 weeks, $P = 0.0063$; 52 weeks, $P = 0.0188$. Data in **a** and **b** are presented as the mean ± s.e.m. $^{*}P < 0.05$, $^{**}P < 0.01$ and $^{***}P < 0.001$; two-way ANOVA with Bonferroni *post hoc* analysis.

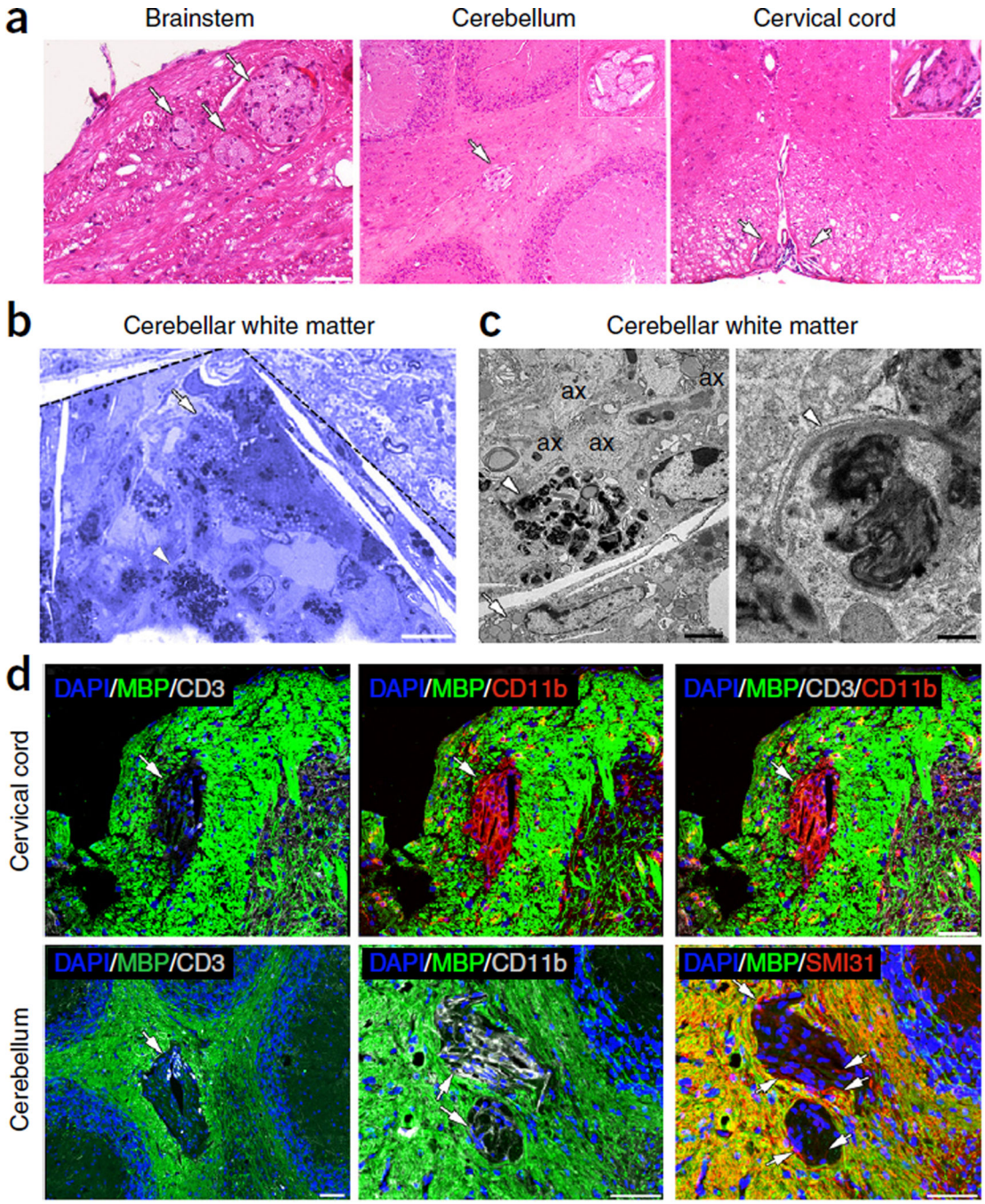

Figure 2.

Focal white matter lesions at early disease stages. (**a**) Focal white matter lesions (arrows) were detected in different CNS areas of the tamoxifen-treated *Plp1-CreER^{T};ROSA26-eGFP-DTA* mice ~40 weeks after injection, such as the brainstem white matter, the cerebellar white matter and the cervical spinal cord white matter. They appear as lighter areas on sections stained with hematoxylin and eosin. Insets show higher magnifications of lesions. Scale bars: 50 μm (brainstem) and 100 μm (cervical cord, cerebellum). (**b,c**) A focal lesion is outlined in the cerebellar white matter (dashed lines) on a toluidine blue–stained section

(**b**). The lesion contains a high density of macrophages with lipids from degrading myelin (arrow) and myelin debris (arrowhead) in their cytoplasm, which are also shown at higher resolution by EM (**c**, left). A higher magnification EM image of the myelin debris is shown in **c**, right. EM analysis also demonstrates the presence of unmyelinated axons (ax) in the focal lesions (**c**, left panel). Scale bars: 10 μm (**b**), 2 μm (**c**, left) and 200 nm (**c**, right). (**d**) Focal lesions showed loss of MBP staining in the cerebellar white matter and the cervical spinal cord white matter (green, arrows), and they frequently contained T cells stained for CD3 (gray). These sites also showed increased staining for the microglia and macrophage marker CD11b (red in cervical cord, gray in cerebellum). A few unmyelinated axons were also detected in the white matter lesions by SMI31 staining (red in cerebellum, arrows). Immunofluorescence images are representative of three mice per genotype. Scale bars, 50 μm.

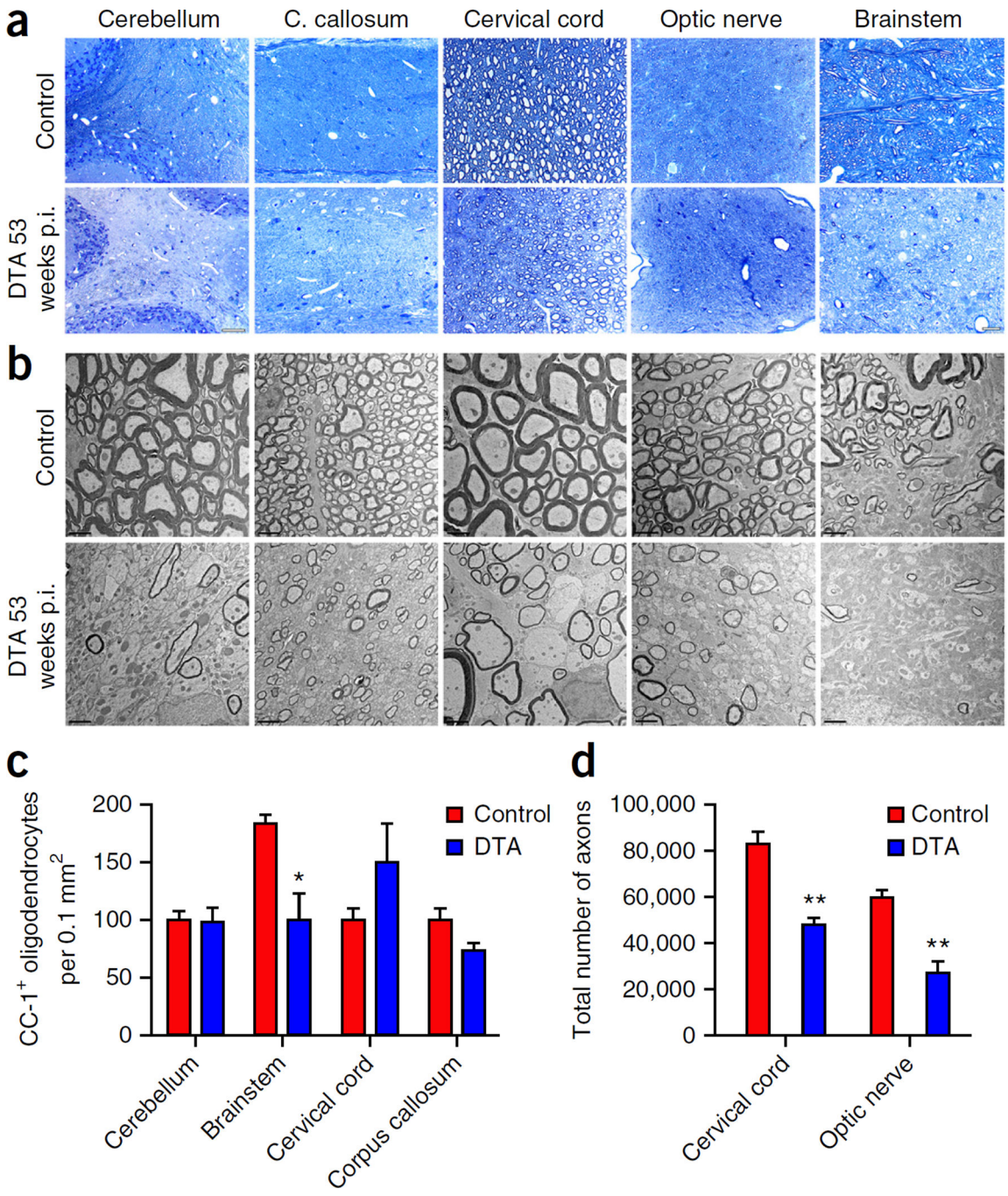

Figure 3.

Extensive myelin and axonal loss at late disease stages. (**a,b**) Toluidine blue staining (**a**) and EM analysis (**b**) showed substantial myelin loss in different CNS white-matter-rich areas of the tamoxifen-treated DTA mice at later disease stages, 53 weeks post-injection (p.i.). Corresponding CNS areas from the control littermate (*ROSA26-eGFP-DTA*) mice are shown in the upper panel. Scale bars: 100 μm (**a**, cerebellum), 20 μm (**a**, corpus (C.) callosum, cervical cord, optic nerve, brainstem) and 2 μm (**b**). Images in **a** and **b** are representative of three mice per genotype. (**c**) Counts of the CC-1-positive cell numbers

indicated significant oligodendrocyte loss in the brainstem of tamoxifen-treated DTA mice at 53 weeks p.i., but not in the cerebellum, cervical cord or corpus callosum, compared with control mice. $N = 3$ mice per genotype (brainstem, cervical cord and corpus callosum), $n = 4$ control mice and $n = 3$ DTA mice (cerebellum). $P = 0.0262$ between control and DTA mice in brainstem. No significance between control and DTA mice: cerebellum, $P = 0.8691$; cervical cord, $P = 0.2245$; corpus callosum, $P = 0.1061$. (**d**) Counts of the total axonal numbers showed significantly fewer axons in the cervical spinal cord ventrolateral white matter and the optic nerve areas of the tamoxifen-treated DTA mice 53 weeks p.i. as compared to control littermate mice. $N = 3$ mice per genotype. Between control and DTA mice: cervical cord, $P = 0.0034$; optic nerve, $P = 0.0024$. Data in **c** and **d** are presented as the mean + s.e.m. $^{**}P < 0.01$, $^{*}P < 0.05$ with two-tailed unpaired Student's *t* test.

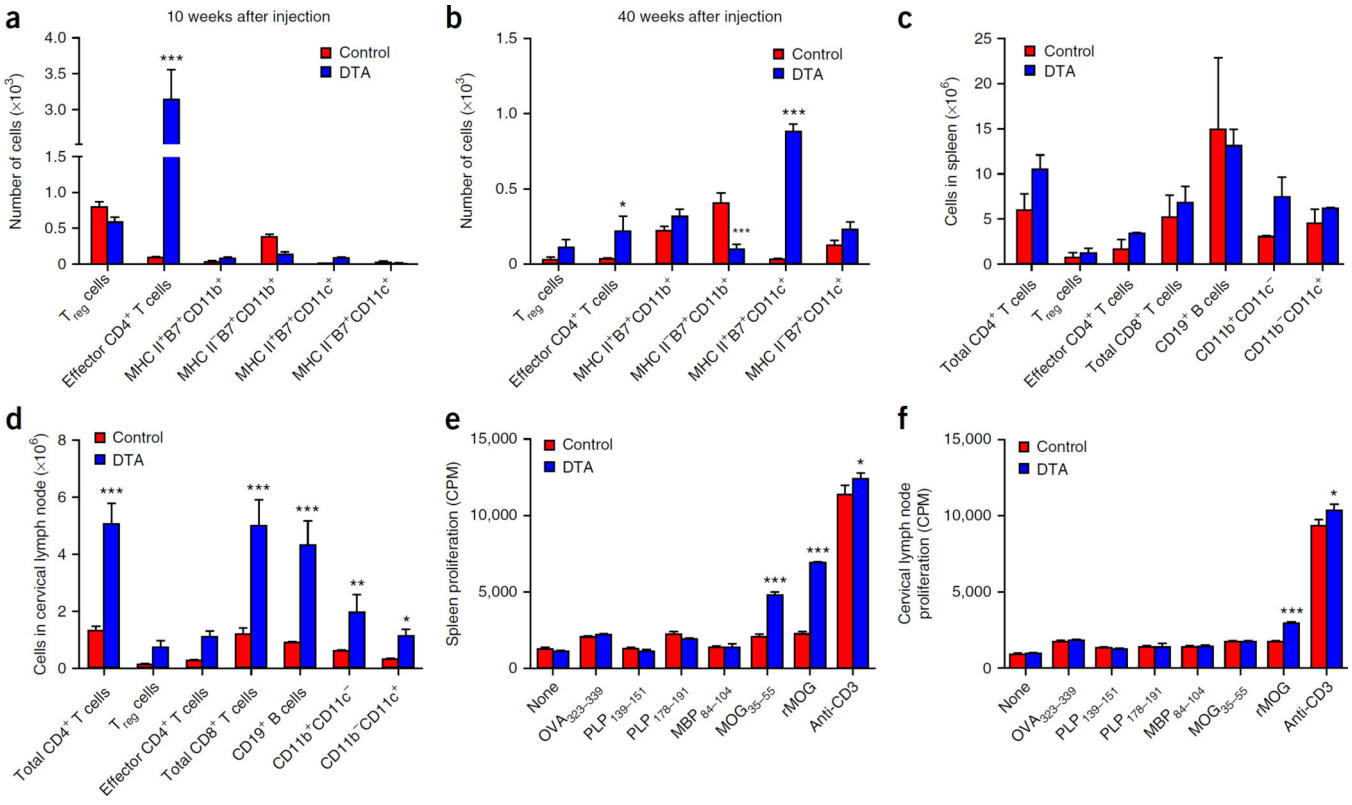

Figure 4.

CNS inflammation and peripheral MOG-specific $CD4^+$ T-cell responses during late-onset demyelination in tamoxifen-treated DTA mice. (**a**) Flow cytometry revealed increased numbers of effector $CD4^+$ T cells ($CD3^+CD4^+CD44^{hi}$) ($P < 0.0001$) in the CNS of the tamoxifen-treated *Plp1-CreER^T;ROSA26-eGFP-DTA* (DTA) mice 10 weeks after injection as compared to the age-matched control *ROSA26-eGFP-DTA* (control) mice ($n = 3$). (**b**) Increased numbers of effector $CD4^+$ T cells ($P = 0.0336$) persisted into late-onset disease at 40 weeks after injection, when the numbers of dendritic cells ($CD3^-CD11b^-CD11c^+$) ($P < 0.0001$) were also increased and $MHCIIB7^+$ monocytes decreased ($P = 0.0005$). (**c,d**) The numbers of total $CD4^+$ T cells ($CD3^+CD4^+CD8^-$) (in cervical lymph nodes, $P = 0.0001$), regulatory T (T_{reg}) cells ($CD3^+CD4^+CD25^+FoxP3^+$), effector $CD4^+$ T cells ($CD3^+CD4^+CD44^{hi}FoxP3^-$), total $CD8^+$ T cells (total $CD3^+CD4^-CD8^+$) (in cervical lymph nodes, $P = 0.0001$), B cells ($CD3^-CD19^+$) (in cervical lymph nodes, $P = 0.0004$), monocytes ($CD3^-CD11b^+CD11c^-$) (in cervical lymph nodes $P = 0.0100$) and dendritic cells ($CD3^-CD11b^-CD11c^+$) (in cervical lymph nodes $P = 0.0267$) were determined by flow cytometry in the spleens (**c**) and cervical lymph nodes (**d**) of tamoxifen-treated DTA mice 40 weeks after injection and control mice. Additionally, splenocytes (**e**) and cervical lymph node cells (**f**) (1×10^6 per well) were activated in culture for 72 h in the presence of medium alone or with anti-CD3 (1 μg/ml) (spleen, $P = 0.0118$; cervical lymph node, $P = 0.012$), $OVA_{323–339}$, $PLP_{139–151}$, $PLP_{178–191}$, $MBP_{84–104}$ or $MOG_{35–55}$ (spleen, $P < 0.0001$) or whole recombinant rat MOG (rMOG) protein (10 μg/ml) (spleen, $P < 0.0001$; cervical lymph node, $P = 0.0005$), with pulsed tritiated thymidine (1 μCi) added at 24 h. The levels of cellular proliferation were then determined. One representative experiment of three is

presented. Three mice from each group were assessed per experiment. The data are presented as the mean + s.e.m. Counts per minute (CPM) of triplicate cultures. $*P < 0.05$, $**P < 0.01$ and $***P < 0.001$ for differences between control mice and tamoxifen-treated DTA mice; two-way ANOVA with Bonferroni *post hoc* analysis.

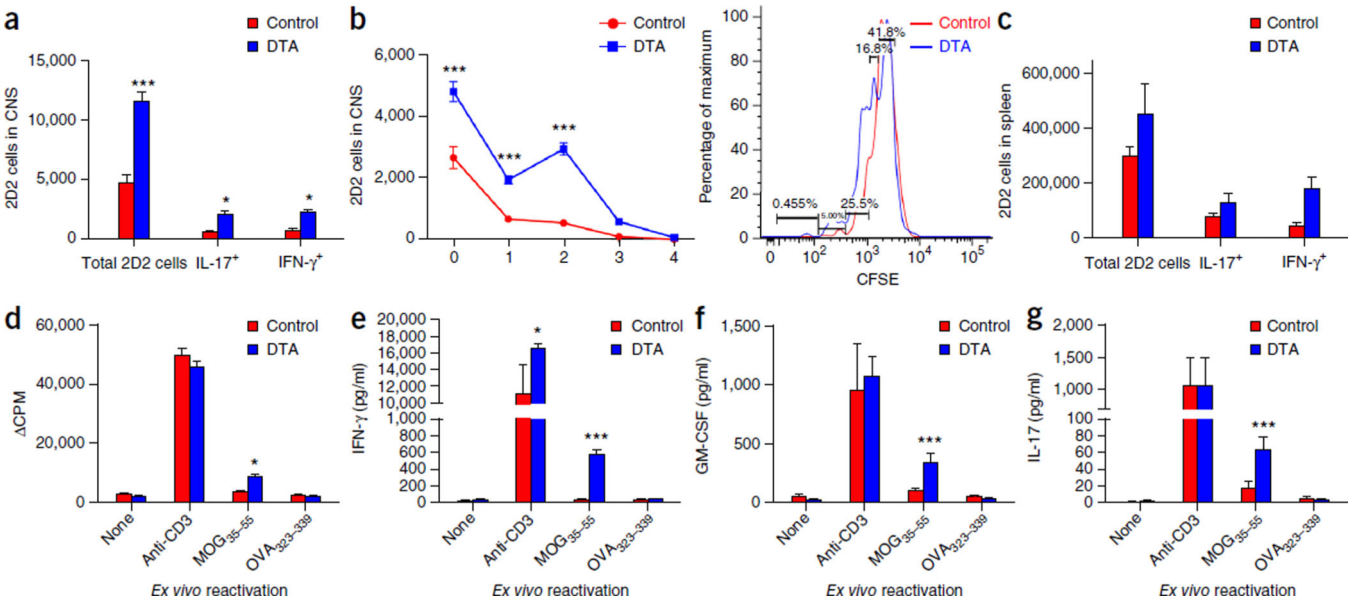

Figure 5.

Activated MOG-specific T cells infiltrate the CNS of the tamoxifen-treated DTA mice during the early demyelinating disease. (**a–g**) CFSE-labeled 2D2 (MOG-specific) T cells were adoptively transferred into tamoxifen-treated *PLP-CreER^T;ROSA26-eGFP-DTA* mice at 7 weeks after injection and into control littermate (*ROSA26-eGFP-DTA*) mice. Flow cytometry was performed 1 week later; it showed increased numbers of proliferating CFSE-labeled 2D2 (MOG-specific) T cells in the CNS ($P < 0.0001$; one representative flow cytometry histogram is presented) (**a,b**), as well as in the spleens of the tamoxifen-treated DTA mice compared to control mice (**c**). Increased numbers of 2D2 cells producing proinflammatory cytokines (IL-17 ($P = 0.0395$) and IFN-γ ($P = 0.0415$)) were also detected in both the CNS (**a**) and the spleens (**c**) of the tamoxifen-treated DTA mice as compared to littermate (control) mice. Furthermore, splenocytes isolated from DTA mice showed increased cellular proliferation (**d**) ($MOG_{35–55}$ activation, $P = 0.0347$), as well as secretion of the proinflammatory cytokines IFN-γ (anti-CD3 activation, $P = 0.0234$; $MOG_{35–55}$ activation, $P < 0.0001$) (**e**), GM-CSF ($MOG_{35–55}$ activation, $P < 0.0001$) (**f**) and IL-17 ($MOG_{35–55}$ activation, $P = 0.0003$) (**g**) when the cells were activated *ex vivo* in the presence of $MOG_{35–55}$. One representative experiment of two is presented with $n = 5$ mice per group. The data are presented as the mean + s.e.m. $*P < 0.05$ and $***P < 0.001$ for differences shown between mice in different groups ($n = 5$); two-way ANOVA with Bonferroni *post hoc* analysis.

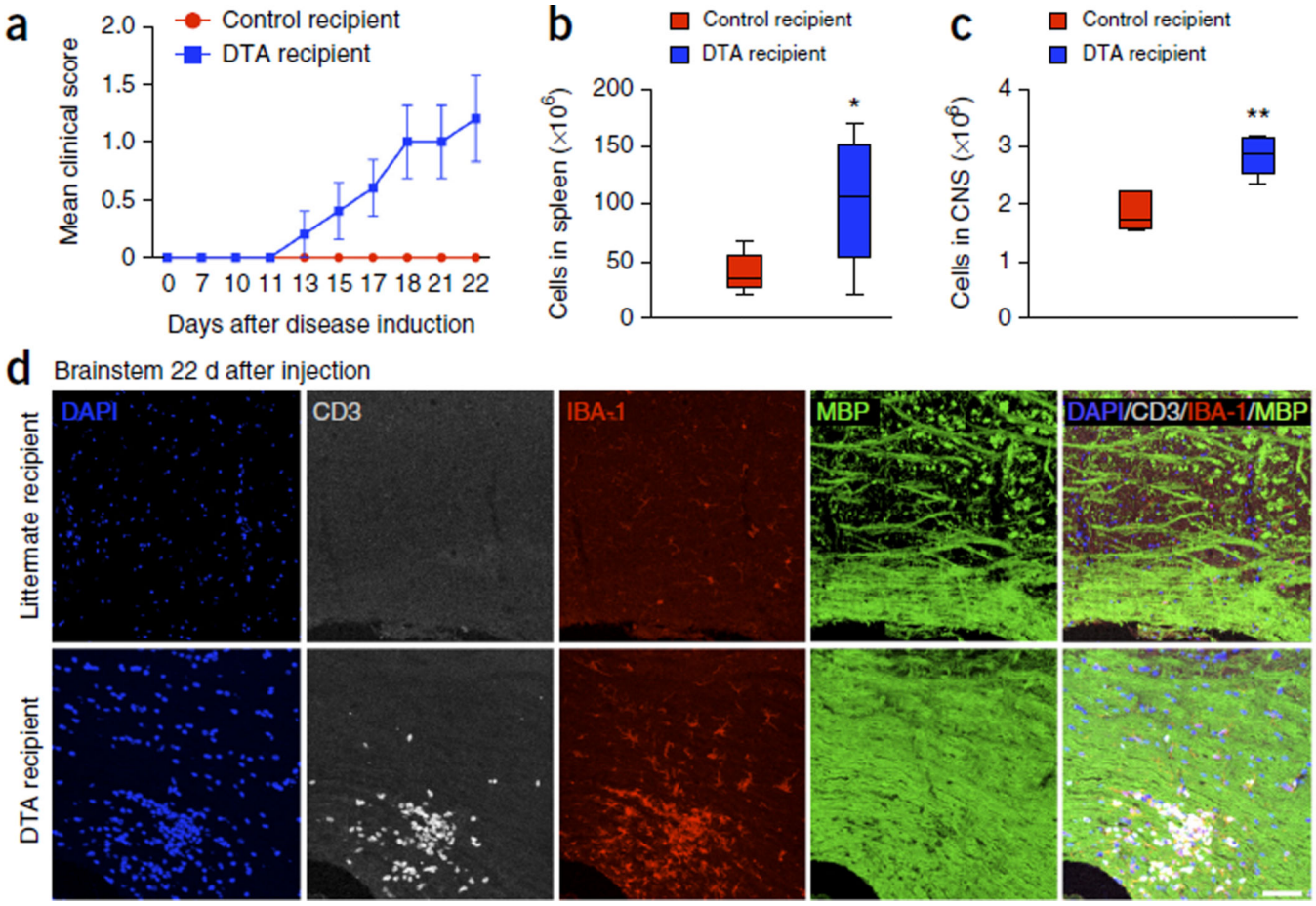

Figure 6.

Adoptive transfer of MOG-specific T cells derived from tamoxifen-treated DTA mice causes white matter inflammation in the CNS of naive *Rag1*$^{-/-}$ mice. One representative experiment of two is presented. Splenic cells from tamoxifen-treated *Plp1-CreER*^{T}*;ROSA26-eGFP-DTA* mice 40–52 weeks after injection or age-matched control (*ROSA26-eGFP-DTA*) mice were cultured for 72 h at in the presence of $MOG_{35–55}$ peptide (20 μg/ml) plus IL-12 (10 ng/ml) and IL-2 (100 U/ml). Cultured cells (10^7 blast cells) from tamoxifen-treated DTA mice were transferred into naive *Rag1*$^{-/-}$ recipient mice. (**a**) Mean (± s.e.m.) EAE scores indicated EAE-like neurological symptoms in *Rag1*$^{-/-}$ mice inoculated with cells from tamoxifen-treated DTA mice (DTA recipient) but not in *Rag1*$^{-/-}$ mice inoculated with cells from littermate mice (control recipient). (**b,c**) On day 22 after cell transfer, the number of total cells present in the spleen (**b**) and CNS (**c**) were enumerated. (**d**) Immunohistochemistry revealed the presence of focal inflammatory lesions with high levels of infiltrating T cells ($CD3^+$ cells, gray) and microglia or macrophages ($IBA\text{-}1^+$ cells, red), without apparent myelin loss (MBP signal, green) in the brainstem of the *Rag1*$^{-/-}$ mice inoculated with T cells from tamoxifen-treated DTA mice (bottom). No white matter lesions were detected in those mice inoculated with cells from control littermate (*ROSA26-eGFP-DTA*) mice (top). Images are representative of five mice per genotype. Scale bar, 60 μm. The data in **a–c** are presented as mean + s.e.m. One representative experiment of two is presented with $n = 5$ mice per group; $^*P < 0.05$, $^{**}P < 0.01$ for differences between control-derived

and DTA-derived cell recipient mice shown in **b** ($P = 0.0398$) and **c** ($P = 0.0016$); one-tailed unpaired Student's *t* test.

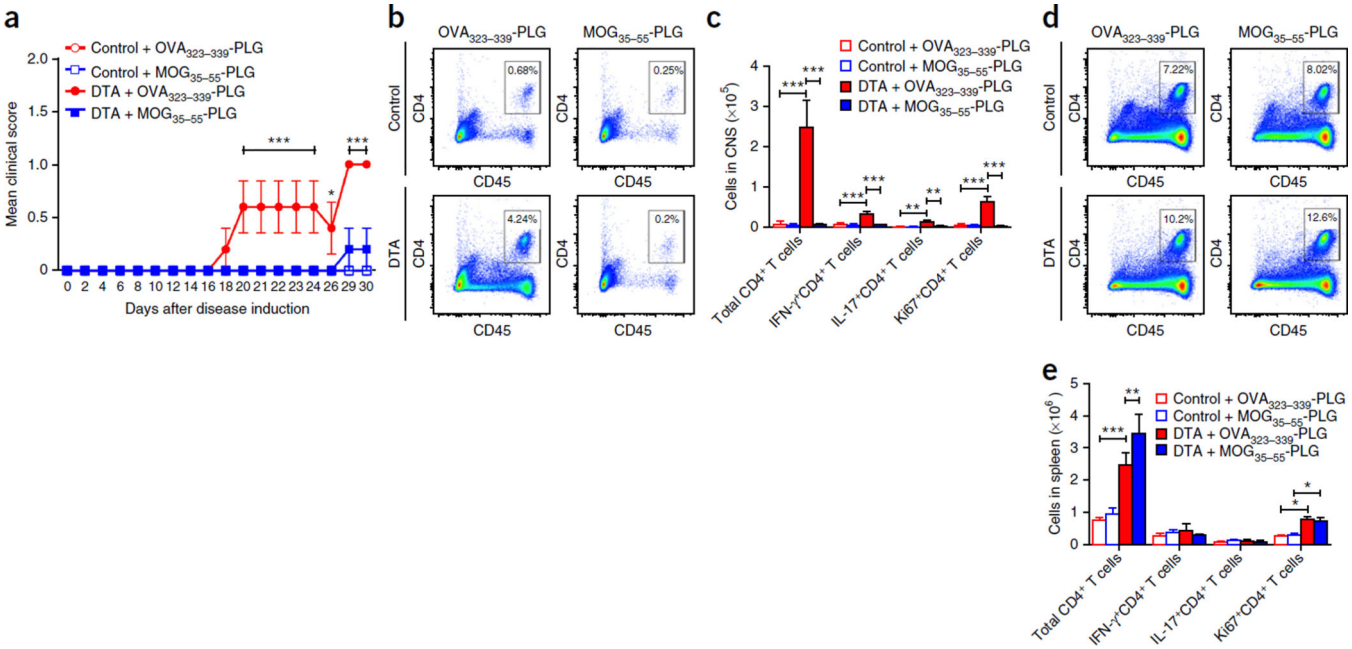

Figure 7.

$MOG_{35–55}$-specific tolerance inhibits CNS entry of DTA mouse-derived $MOG_{35–55}$-specific T cells. As in Figure 6, $MOG_{35–55}$-activated blast cells were generated from tamoxifen-treated *Plp1-CreER^T;ROSA26-eGFP-DTA* and control (*ROSA26-eGFP-DTA*) mice. Recipient *Rag1*$^{-/-}$ mice received control-derived or DTA-derived blast cells plus either $OVA_{323–339}$-PLG or $MOG_{35–55}$-PLG nanoparticles via i.v. injection ($n = 5$). (**a**) The recipient mice were followed for disease (DTA + $MOG_{35–55}$-PLG compared to DTA + $OVA_{323–339}$-PLG: $P < 0.0001$, days 20–24 and days 29–30; $P = 0.0331$, day 26) and, on day 30 after cell transfer, spleen and CNS samples were assayed for the number and phenotype of the CD4$^+$ T cells present. (**b**) Analysis of representative CNS samples gating on total singlet live CD45^{hi}CD4$^+$ cells. (**c**) This population of CD4$^+$ T cells was further analyzed to determine the number of T cells that were CD4$^+$ (control + $OVA_{323–339}$-PLG compared to DTA + $OVA_{323–339}$-PLG, $P < 0.0001$; DTA + $OVA_{323–339}$-PLG compared to DTA + $OVA_{323–339}$-PLG, $P < 0.0001$), IFN-γ$^+$CD4$^+$ (control + $OVA_{323–339}$-PLG compared to DTA + $OVA_{323–339}$-PLG, $P < 0.0001$; DTA + $OVA_{323–339}$-PLG compared to DTA + $OVA_{323–339}$-PLG, $P < 0.0001$), IL-17$^+$CD4$^+$ (control + $OVA_{323–339}$-PLG compared to DTA + $OVA_{323–339}$-PLG, $P \leq 0.0032$; DTA + $OVA_{323–339}$-PLG compared to DTA + $OVA_{323–339}$-PLG, $P = 0.0032$), and Ki67$^+$CD4$^+$ (control + $OVA_{323–339}$-PLG compared to DTA + $OVA_{323–339}$-PLG, $P < 0.0001$; DTA + $OVA_{323–339}$-PLG compared to DTA + $OVA_{323–339}$-PLG, $P < 0.0001$). Representative flow plots are presented in Supplementary Figure 8a–c. (**d**) Analysis of representative spleen samples gating on total singlet live CD45^{hi}CD4$^+$ cells. (**e**) This population of CD4$^+$ T cells was further analyzed to determine the number of T cells that were CD4$^+$ (control + $OVA_{323–339}$-PLG compared to DTA + $OVA_{323–339}$-PLG, $P < 0.0001$; DTA + $OVA_{323–339}$-PLG compared to DTA + $OVA_{323–339}$-PLG, $P = 0.0099$), IFN-γ$^+$CD4$^+$, IL-17$^+$CD4$^+$, and Ki67$^+$CD4$^+$ (control + $OVA_{323–339}$-PLG compared to DTA + $OVA_{323–339}$-PLG, $P = 0.02$; DTA + $OVA_{323–339}$-PLG compared to DTA + $OVA_{323–339}$-PLG, $P = 0.009$). One representative experiment of two is presented with $n = 5$ mice per group.

Representative flow plots are presented in Supplementary Figure 8d–f. The data are presented as mean + s.e.m. $*P < 0.05$, $**P < 0.01$ and $***P < 0.001$ for differences shown between mice in different groups; two-way ANOVA with Bonferroni *post hoc* analysis.

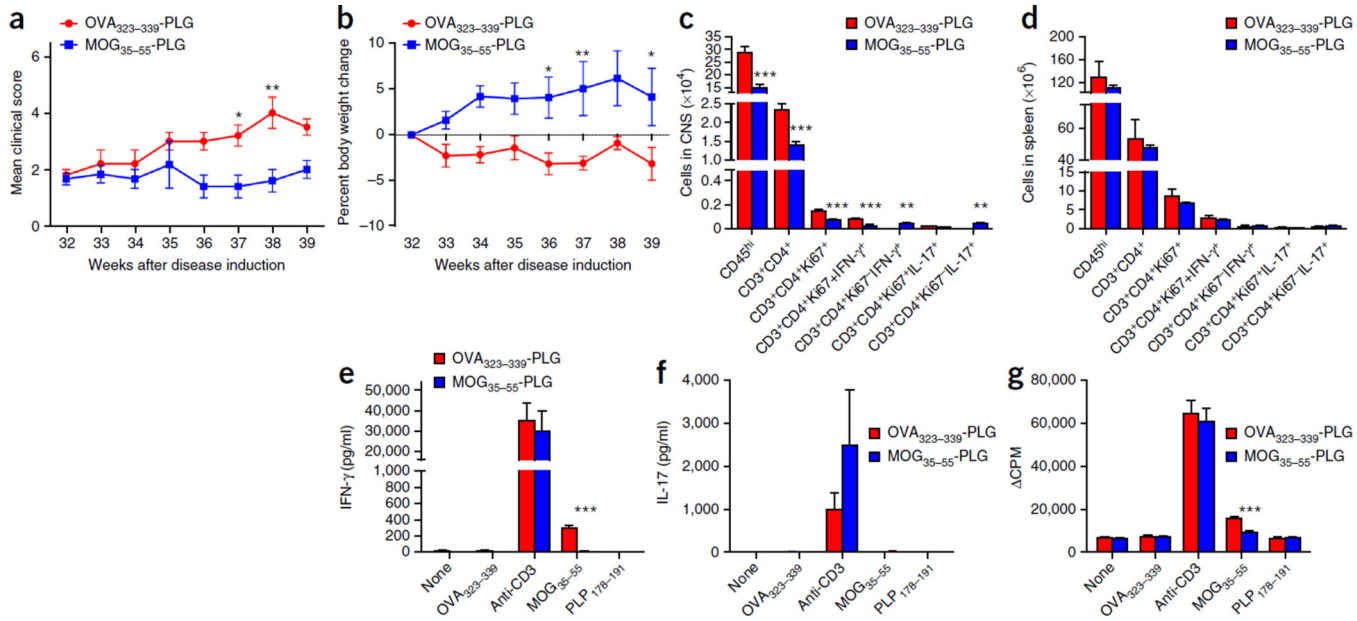

Figure 8.

Tolerance against $MOG_{35–55}$ inhibits neurological disease induced by the DTA-derived MOG-specific T cells. Tamoxifen-treated *Plp1-CreER^T;ROSA26-eGFP-DTA* mice at 32 weeks after injection were either tolerized against the $MOG_{35–55}$ peptide by a single i.v. treatment with $MOG_{35–55}$-PLG nanoparticles or injected with control $OVA_{323–339}$-PLG nanoparticles. (**a**) Motor defects (DTA + $OVA_{323–339}$-PLG compared to DTA + $MOG_{35–55}$-PLG: week 37, $P = 0.0393$; week 38, $P = 0.0019$) and (**b**) weight loss were assessed weekly between weeks 32 and 39 (DTA + $OVA_{323–339}$-PLG compared to DTA + $MOG_{35–55}$-PLG: week 36, $P = 0.0281$; week 37, $P = 0.009$; week 39, $P = 0.0434$). (**c,d**) At week 39 after injection, FACS analysis of the CNS (**c**) ($CD45^{hi}$, $P < 0.0001$; $CD3^+CD4^+$, $P < 0.0001$; $CD3^+CD4^+Ki67^+$, $P < 0.0001$; $CD3^+CD4^+Ki67^+IFN\text{-}\gamma^+$, $P < 0.0001$; $CD3^+CD4^+Ki67^-IFN\text{-}\gamma^+$, $P = 0.009$; $CD3^+CD4^+Ki67^-IL\text{-}17^+$, $P = 0.009$) and spleens (**d**) was completed to determine the number and phenotype of the $CD4^+$ T cells in these tissues. (**e–g**) $CD4^+$ T cell responses to $MOG_{35–55}$ were assessed by culturing 1×10^6 total splenocytes for 3 d with medium alone, anti-CD3 (1 μg/ml), $OVA_{323–339}$, $MOG_{35–55}$ or $PLP_{178–191}$ (10 μg/ml). The levels of secreted IFN-γ (**e**) ($MOG_{35–55}$ activation $P < 0.0001$), IL-17 (**f**) and cellular proliferation (**g**) ($MOG_{35–55}$ activation $P < 0.0001$) as determined by tritiated thymidine incorporation were assessed. One representative experiment of two is presented with $n = 6$ mice per group. The data are presented as the mean + s.e.m. $^*P < 0.05$, $^{**}P < 0.01$ and $^{***}P < 0.001$ for differences shown between the different groups. Two-way ANOVA with Bonferroni *post hoc* analysis.